Am J Physiol Heart Circ Physiol 285: H2531–H2542, 2003.
First published July 31, 2003; 10.1152/ajpheart.00381.2003.

Behavior of ectopic surface: effects of β-adrenergic stimulation and uncoupling

Ara Arutunyan,[1] Alain Pumir,[2] Valentin Krinsky,[2] Luther Swift,[1] and Narine Sarvazyan[1]
[1]*Department of Physiology, Texas Tech University Health Sciences Center, Lubbock, Texas 79430; and* [2]*Institut Non-Linéaire de Nice, Centre National de la Recherche Scientifique, F-06560 Valbonne, France*

Submitted 24 April 2003; accepted in final form 25 July 2003

Arutunyan, Ara, Alain Pumir, Valentin Krinsky, Luther Swift, and Narine Sarvazyan. Behavior of ectopic surface: effects of β-adrenergic stimulation and uncoupling. *Am J Physiol Heart Circ Physiol* 285: H2531–H2542, 2003. First published July 31, 2003; 10.1152/ajpheart.00381.2003.—By using both experimental and theoretical means, we have addressed the progression of ectopic activity from individual cardiac cells to a multicellular two-dimensional network. Experimental conditions that favor ectopic activity have been created by local perfusion of a small area of cardiomyocyte network (I-zone) with an isoproterenol-heptanol containing solution. The application of this solution initially slowed down and then fully blocked wave propagation inside the I-zone. After a brief lag period, ectopically active cells appeared in the I-zone, followed by evolution of the ectopic clusters into slowly propagating waves. The changing pattern of colliding and expanding ectopic waves confined to the I-zone persisted for as long as the isoproterenol-heptanol environment was present. On restoration of the control environment, the ectopic waves from the I-zone broke out into the surrounding network causing arrhythmias. The observed sequence of events was also modeled by FitzHugh-Nagumo equations and included a cell's arrangement of two adjacent square regions of 20 × 20 cells. The control zone consisted of well-connected, excitable cells, and the I-zone was made of weakly coupled cells (heptanol effect), which became spontaneously active as time evolved (isoproterenol effect). The dynamic events in the system have been studied numerically with the use of a finite difference method. Together, our experimental and computational data have revealed that the combination of low coupling, increased excitability, and spatial heterogeneity can lead to the development of ectopic waves confined to the injured network. This transient condition appears to serve as an essential step for the ectopic activity to "mature" before escaping into the surrounding control network.

zone; cardiac arrhythmia; functional border zone; ischemia-reperfusion injury

THE PROCESS of how an ectopic source leads to an arrhythmia remains the subject of intensive investigations. Specifically, theoretical studies have demonstrated the critical role of the size of an automatic focus (14) as well as partial uncoupling (13) in the propagation of activity from the focus into surrounding myocardium and predicted that the presence of anisotropy facilitates the spread of focal activity (18, 37). The Luo-Rudy model of the ventricular myocyte in a multicellular fiber was used to show that L-type Ca^{2+} current plays a major role in sustaining conduction when structural inhomogeneity is present or intercellular coupling is reduced (31, 36). Numerous studies in single cells have shown spontaneous depolarization and the appearance of triggered activity under β-adrenergic stimulation, Ca^{2+} overload, or reperfusion-like conditions (10). A recent theoretical study (26) has also pointed to an essential role of intermediate uncoupling in propagation of triggered activity from the ischemic area. Thus the conditions that favor origination of ectopic activity have been largely understood. At the same time, the process that allows ectopic activity to progress into a large-scale arrhythmia remains elusive. Our study attempts to give some insights into this process.

To visualize how the activity from individual ectopic sources propagates, we have used a recently developed experimental model, which allows one to create a localized area of injury (termed I-zone) and to monitor the development of arrhythmias within a two-dimensional (2D) network of cardiac cells (4). To create an injury we have employed a local application of a β-adrenergic agonist isoproterenol (Iso) and a gap-junctional uncoupler heptanol (Hept). The use of Hept in our experiments allowed us to mimic progressive uncoupling known to occur during ischemia. In vivo, this process has been linked to a variety of factors, including increases in intracellular Ca^{2+} (Ca_i^{2+}) and H^+ concentrations (11, 17), accumulation of amphipathic lipid metabolites (24, 38), and changes in phosphorylation levels of connexins (6). The use of Iso, on the other hand, allowed us to simulate the massive release of endogenous catecholamines known to occur during myocardial ischemia (20). Notably, the levels of interstitial norepinephrine have been shown to increase progressively in the ischemic areas, whereas dialysate from nonischemic regions showed no significant changes (2). Such a local surge of catecholamines resembles the conditions of our experimental model, where a small area of the myocyte network is perfused with Iso. Besides mimicking endogenous catecholamine release, Iso application also served as a general

Address for reprint requests and other correspondence: N. Sarvazyan, Physiology Dept., Texas Tech Univ. Health Sciences Center, 3601 4th St., Lubbock TX 79430 (E-mail: Narine.Sarvazyan@ttuhsc.edu).

The costs of publication of this article were defrayed in part by the payment of page charges. The article must therefore be hereby marked "*advertisement*" in accordance with 18 U.S.C. Section 1734 solely to indicate this fact.

means to increase the spontaneous depolarization rate of a myocyte, which in vivo was linked to multiple factors, including Ca^{2+} overload, injury currents, and inhibition of potassium conductance (10).

In our previous report (3), we observed ectopic arrhythmias during washout of the ischemia-like solution. The ischemic solution in that study included Hept, elevated potassium, low pH, and other components of the ischemic milieu. The process, which led from individual ectopic events to the full-scale arrhythmia, originated mostly at the border of the I-zone and was transient as it occurred during just the first few seconds of reperfusion. Therefore, characterization and modeling of the ectopic process progression was hardly feasible. To overcome these limitations, we decided to substitute a short-lived increase in cell excitability associated with reperfusion with a more reliable experimental intervention. Indeed, a combined application of Iso and Hept to the I-zone has allowed us to extend, both in time and space, the fleeting condition that appears to "breed" ectopic arrhythmias. We then characterized temporal features of the ectopic process, including its individual phases and modeled such behavior theoretically. Together, our data have shown that combination of low coupling, increased excitability, and spatial heterogeneity leads to the development of ectopic waves confined to the injured network. This transient condition served as an essential step for the ectopic activity to mature before escaping into the surrounding control network.

MATERIALS AND METHODS

Myocyte culture. Cardiomyocytes from 2-day-old Sprague-Dawley rats were obtained using enzymatic digestion procedure (4) in accordance with the guidelines of the Texas Tech University Health Sciences Center Animal Care and Use Committee. The cells were plated on 25-mm laminin-coated glass coverslips (10^5 cells/cm^2) and kept under standard culture conditions in Dulbecco's modified minimum essential medium supplemented with 5% FBS, 10 U/ml penicillin, 10 μg/ml gentamicin, and 1 μg/ml streptomycin. To determine the purity of the cultures, cells were stained for sarcomeric myosin with the use of primary antibodies from Developmental Studies Hybridoma Bank, as described previously (4). By the third day in culture, the cells had formed interconnected confluent networks that exhibited rhythmic, spontaneous contractions and could be used in experiments for an additional 3 or 4 days. To create partitions within the cell layer we employed a 0.5-mm flat-tip needle to remove cells from the designated areas.

Experimental chamber. We used a custom-made experimental chamber that allows one to perfuse a small area of cell network with a solution of interest, while observing events under the microscope. Hydrodynamics and temporal characteristics of flow, as well as the chamber's detailed design, have been described earlier (4). In brief, the chamber consisted of a stainless steel holder for mounting a glass coverslip and a Plexiglas base that contained two inlets and one outlet (Fig. 1*A*). Two platinum electrodes embedded in the top of the chamber were used to stimulate a small cluster of myocytes immediately below and the excitation then spread through the rest of network with 10–17 cm/s propagation velocity. To determine the excitation threshold, we applied monophasic 1.2-ms pulses starting at 0.4 V/cm and then increased the stimuli in 0.1-V increments until each pacing pulse was followed by a Ca^{2+} transient (CaT) wave. The monolayer, which behaved as a syncytium, was then continuously paced at 0.2–0.5 Hz by a voltage 20% higher than the excitation threshold (average threshold values were 0.8 V/cm). Experiments were conducted at 25°C as justified previously (3, 4).

Recording of ectopic waves. To visualize the propagation of ectopic activity, we recorded CaT instead of membrane potentials. Voltage-sensitive dyes were not employed because these indicators exhibit a <10% change of emission intensity in response to an action potential (as compared with a 10-fold increase in fluo 4 intensity associated with CaT). Such limited dynamic range renders potentiometric indicators unsuitable for experiments that require low magnification objectives to visualize the unpredictable occurrence of ectopic foci in a 2D multicellular network because these objectives collect only a limited amount of emitted light due to their low numerical apertures. In addition, rapid photobleaching of potentiometric dyes together with the toxicity of their oxidation products (29) makes them unsuitable for the continuous acquisition (>30 min) used in our studies. Thus we employed CaT recordings, which have been used successfully to monitor impulse propagation both in cell culture (3, 8) and on the whole heart level (21).

Monitoring CaTs. Cells plated on laminin-covered coverslips were loaded with 5 μM Fluo-4AM for 1 h. Each spontaneous or paced action potential was associated with an increase in Ca_i^{2+} recorded as a CaT. Notably, the motion artifacts are negligible when one acquires a signal from a large field of cells, such as the regions of interests used in our study. Fluo-4 was excited at 488 nm, and the fluorescence was acquired at wavelengths of >515 nm. Experiments were conducted in two modes: *x-y* and *x-t* (linescan). The two modes complemented each other, aiding in one's understanding of the events associated with ectopic activity. The *x-y* mode (128 × 128 pixels, 166 ms/frame) was used to monitor the developing 2D pattern of propagating CaT waves. The linescan mode allowed the recording of CaT from individual cells with a 6-ms temporal resolution (typical linescan consisted of 1,024 lines, 6 ms/line). Figure 1*B* illustrates the two modes of data acquisition.

Acquisition system. Cells were imaged with the use of a Bio-Rad laser scanning confocal system (model MRC-1024 interfaced to an Olympus IX-70 inverted microscope) with low-power magnification objective (Olympus PlanApo 4×/0.16 numerical aperture) to capture the injury and control zones simultaneously (Fig. 1*B*). Notably, low-magnification objectives have large depths of field, and use of confocal imaging system removes interfering signals from the plastic part of the chamber, displaying only a thin optical section from the focal plane where the cells are found. Another advantage of the employed imaging system was minimization of the light exposure (as a result of sequential, point-by-point laser scanning of the sample), which allowed us to continuously acquire data (for up to 2 h) without significant cell damage and probe bleaching (3).

Experimental protocols. All solutions were equilibrated with atmospheric oxygen. Initially, cells were superfused for 10–20 min with a control Tyrode solution supplemented with 10 mM HEPES pH 7.3 (300 mosM). To simulate conditions that promote ectopic activity, cells within the I-zone were superfused with Tyrode containing Hept and Iso. A typical protocol consisted of 10 min of perfusion with Tyrode, followed by a 5-min perfusion of the I-zone cells with Tyrode, containing either 5 μM Iso, 2 mM Hept, or 5 μM Iso + 2 mM

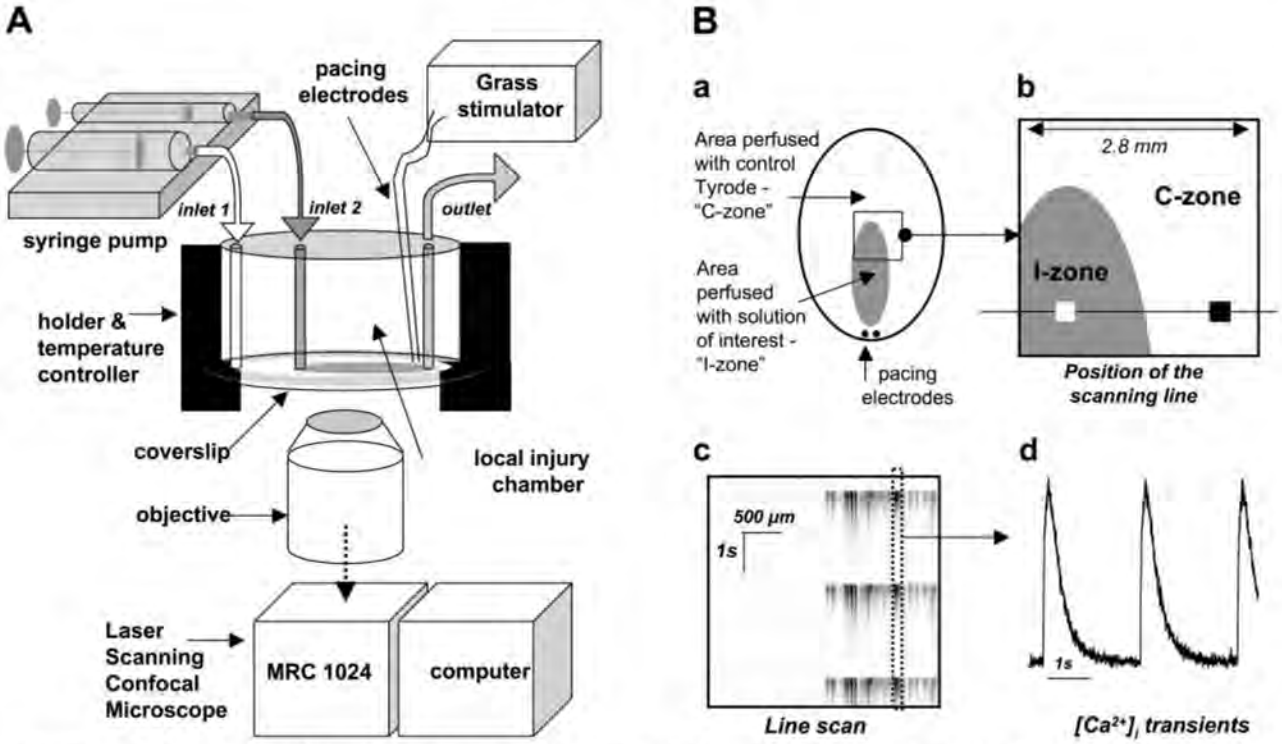

Fig. 1. Diagram of general setup (*A*) and acquisition settings (*B*). *A*: solutions are delivered to two inlets by an automated multisyringe pump. The chamber is placed inside a Peltier temperature-controlled mount, and cells are observed in an inverted mode using a Bio-Rad model MRC-1024 confocal imaging system. *B*, *a*: shape and position of the I-zone (depicted in gray) and pacing electrodes. *b*, Square region typically used for *x*-*y* acquisition. White and black squares show respective positions of the two regions from which I-zone and C-zone traces were acquired. Horizontal line indicates position of the laser beam when experiments were conducted in *x*-*t* mode. In this mode fluorescence intensity values were collected along a fixed *x*-line every 6 ms and the lines are plotted sequentially, forming an *x*-*t* image. *c*, Sample *x*-*t* image that shows appearance of the Ca^{2+} transient (CaT) in the control area only (*right*). Cells in the injury zone are silent (*left*). *d*, Individual CaT trace derived from the *x*-t image shown in *c* (black dotted rectangle). $[Ca^{2+}]_i$, intracellular Ca^{2+} concentration.

Hept. Washout of these solutions from the I-zone by the control Tyrode constituted reperfusion. Pacing was applied continuously throughout the entire duration of the experiment [pacing electrodes were located in the control Tyrode zone (C-zone) as shown in Fig. 1*B*].

Numerical study of cardiac network behavior. Experiment-derived conclusions regarding the role of macroscopic parameters (coupling and cell excitability) have been confirmed using a generic FitzHugh-Nagumo (FHN) model of cardiac cell. FHN describes the qualitative aspects of excitation and propagation while lumping together the various slow currents (15). Specifically, the FHN model describes the state of a cell by a variable, e, related to the membrane potential, in such a way that $e = 0$ corresponds to the resting state, and $e = 1$ corresponds to the fully depolarized state, and by the variable ω, representing the total slow current. These variables conform to the following differential equations

$$de/dt = f(e) - \omega + (\text{coupling term}) \quad (1)$$

$$d\omega/dt = \varepsilon(e - \omega - \alpha) \quad (2)$$

The parameter ε is small ($\varepsilon = 0.01$), reflecting the fact that the dynamics of ω is much slower than the dynamics of e. de/dt is the time derivative. The function $f(e)$ has an inverted N shape, and in this study we represented it by the cubic function $f(e) = e\,(1 - e)\,(e - 0.1)$. The parameter α in *Eq. 2* is related to an ectopic activity of the cell (e.g., automaticity) (15). A small value of α implies that the cell is nonoscillatory: a linearly stable quiescent state exists around $e = 0$. A perturbation of amplitude larger than the excitation threshold, however, triggers an action potential. The smaller the α, the larger the excitation threshold, therefore the more difficult it is to drive the system away from the quiescent state. For larger values of α, the quiescent stable state around $e = 0$ disappears and the cell becomes spontaneously oscillatory.

We consider an idealized situation, where cells are located on a square lattice, so the variables are labeled by two integers, i and j, referring to the rows and columns of the lattice. The coupling term in *Eq. 1* describes the electrical conduction between neighboring cells as

$$\text{coupling term } (i,j) = D(e_{i+1,j} + e_{i-1,j} + e_{i,j+1} - e_{i,j-1} - 4e_{i,j}) \quad (3)$$

The coefficient D is proportional to the conductivity between cells. Geometrically, we consider a cell's arrangement, consisting of two square regions of 20×20 cells each, adjacent to each other. The unit length in our system corresponds to 30 μm. Our numerical system thus represents a physical rectangle of 0.6 mm × 1.2 mm. The C-zone consists of strongly coupled ($D = 10$) excitable cells. In the I-zone, the action of Hept is modeled by a reduction of the coupling term D to 0.01 (for the purpose of modeling the perfusion/washout process, the unit time scale in the model defined by *Eqs. 1* and *2* is interpreted to be 0.1 s). The action of Iso is represented by an increase of the parameter α, thus driving the cell toward an

oscillatory state. For each cell, the value of α is assumed to respond as a function of time according to

$$\alpha(i; j; t) = \alpha_0(i; j) f_\alpha(t) \quad (4)$$

To represent cellular heterogeneity, we assume that the value of $\alpha_0(i; j)$ is randomly distributed. The results reported here are obtained with a Gaussian distribution of $\alpha_0 = 0.11 \pm 0.05$. This corresponds to a distribution of periods of the oscillating cells in the range of 9.7–13.6 s. During the application of Iso-Hept solution, the function f_α grows from 0 to 1 in a time of order 300 s. On washout, the value of f_α returns to 0 with a characteristic time of 150 s. To mimic the pacing applied experimentally, we added numerically an external periodic current at the edge of the C-zone, which generated a train of periodic waves.

The system was studied numerically with the use of a finite difference method. We used either a Crank-Nicholson or a second-order Runge-Kutta scheme. These schemes are second order in space and time (27). The time step was chosen by making sure that the numerical results did not change when diminishing the time step by a factor two.

Data analysis. Each of the experimental protocols was conducted at least seven times. Presented figures and graphs are typical results of corresponding scenarios. Quantitative results are expressed as means ± SD. Data and images were plotted using Microcal Origin version 6.0 and NIH Image software (Scion).

Chemicals. Collagenase type II was obtained from Worthington (Freehold, NJ). Culture medium and porcine trypsin were obtained from GIBCO-BRL (Grand Island, NY). Fluo-4-AM was purchased from Molecular Probes (Eugene, OR). Fetal bovine serum (FBS), Tyrode solution, and all other chemicals were purchased from Sigma (St. Louis, MO).

RESULTS

Local perfusion with Hept-containing Tyrode solution. Heptanol is a widely used reversible inhibitor of cell-to-cell coupling (1, 8). In neonatal rat cardiomyocytes, the 2 mM concentration of Hept reversibly inhibits gap-junctional permeability (9, 33), whereas its effect on Ca_i^{2+} and spontaneous contractions is negligible (5, 16). In our experiments, the application of 2 mM Hept caused the rapid disappearance of CaT in the I-zone (24.1 ± 6.3 s, $n = 7$). Cells remained silent for the duration of Hept perfusion (up to 30 min; data not shown). The effect of Hept on CaT was reversible because the frequency and amplitude of CaT returned to the control levels after the removal of Hept (Fig. 2). Whereas Hept reversibly suppressed CaTs within I-zone, no disturbances of the rhythm in the control area were recorded either during Hept application or its washout.

Figure 3 illustrates that the absence of CaT in the I-zone during Hept application also indicates a failure of action potential propagation, not just suppression of CaTs. The experiment was performed in a mechanically partitioned cell monolayer. It shows that application of Hept to the I-zone prevents passage of the paced CaT to the adjacent part of the control network. If electrical activity were to be present in the I-zone during Hept application, it would lead to the resumption the pacing CaT pattern on the other side of the control network, which is contrary to the observed data. The substitution of Hept with another gap-junc-

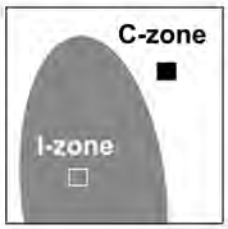

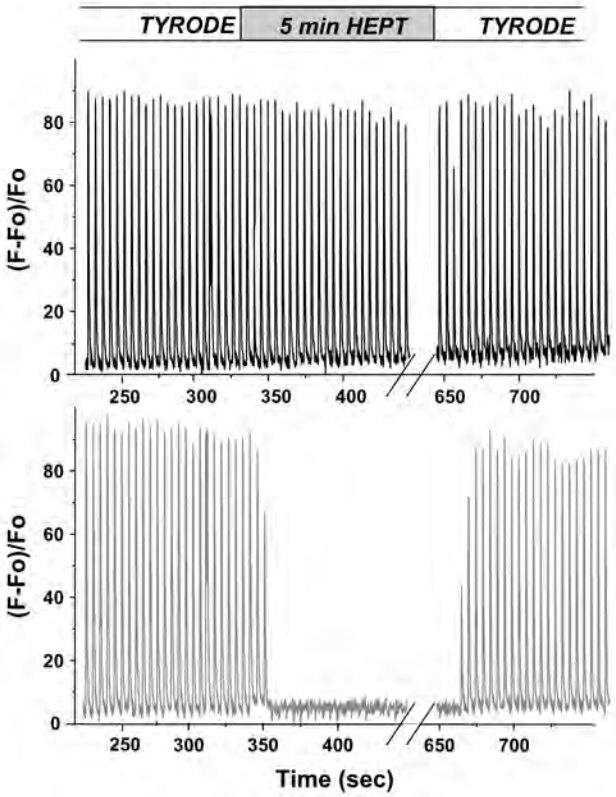

Fig. 2. Effect of local perfusion with heptanol (Hept) on rhythmic pattern of CaT elicited by pacing electrodes. Traces from the representative experiment with Hept show the disappearance and restoration of the CaT from the I-zone. Diagram on the left shows the shape of the I-zone and position of the two regions of interest from which traces were acquired (gray, I-zone; black, control). Fo, baseline fluorescence intensity [(F − Fo)/Fo, the relative change in fluorescence].

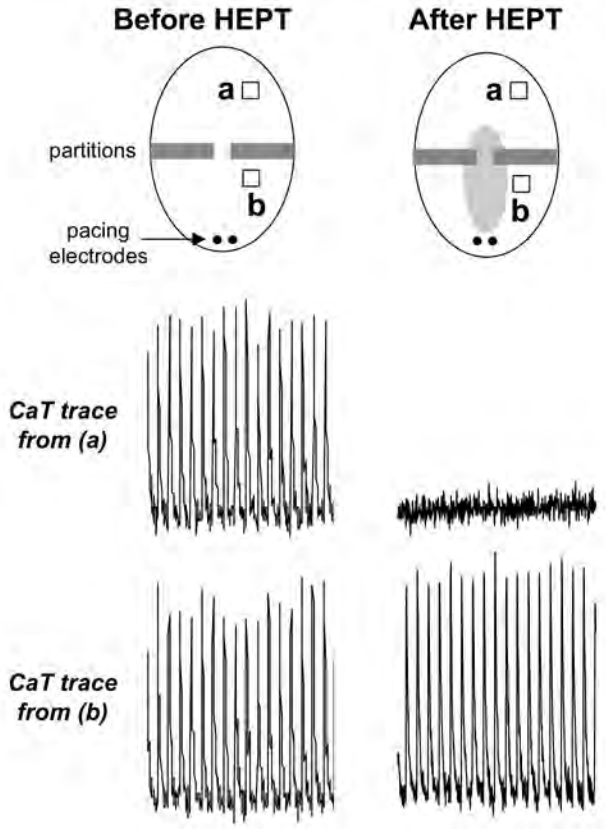

Fig. 3. Local perfusion with Hept inhibits the propagation of paced activity. The cells were mechanically removed from the areas marked as partitions. The myocyte network was paced using a pair of electrodes, and CaTs were recorded from two regions marked as *a* and *b*. After 2 mM Hept was applied to the I-zone, and the CaT from the region *a* disappeared. If one assumes that waves of electrical activity are passing through the I-zone, it will lead to reappearance of the CaT in the *a* region (located in the C-zone), where cells are continuously perfused with the control Tyrode solution. However, the opposite situation is observed, indicating that the absence of CaT in the I-zone during Hept application indicates a failure of action potential propagation, not just suppression of CaTs.

tional uncoupler, palmitoleic acid (28), led to similar results. Specifically, local perfusion with 20 μM palmitoleic acid inhibited propagation of the paced activity to the I-zone, followed by the restoration of CaT pattern on uncoupler removal (data not shown).

Local perfusion with Iso-containing Tyrode solution. Short-term application of 5 μM Iso to the I-zone led to a small increase in CaT amplitude (12.6 ± 5.0% of the initial value). We have also observed shortening of CaT due to a 17% decrease in the half-time ($t_{1/2}$) of CaT decay (from 0.32 ± 0.06 to 0.28 ± 0.07 s). Both effects are in accordance with previous studies, which tested the effect of Iso on isolated myocytes from neonatal rats (19). Aside from these effects on individual CaT, perfusion with Iso did not alter the general pattern of CaT propagation across the myocyte network. Specifically, with the exemption of an occasional double CaT, due to known capacity of Iso to induce early afterdepolarizations (39), no arrhythmias were detected during either perfusion or on washout of 5 μM Iso.

General sequence of events during local perfusion with Iso-Hept-containing Tyrode solution. The combined application of Iso-Hept resulted in the behavior of a network that was markedly different from the experiments when either Hept or Iso alone were present. It led to a prominent arrhythmia-like response in both the I-zone and the control area (Fig. 4). Although the process was essentially continuous, we have divided it into phases for quantification and description purposes. Specifically, based on the results acquired from both *x-y* and linescan experiments (Figs. 4–7) events were classified into the five subsequent phases: *phase I*, slowing of CaT wave propagation inside the I-zone; *phase II*, period of quiescence; *phase III*, appearance of ectopics and ectopic clusters; and *phase IV*, evolution of small ectopic clusters into local CaT waves confined to the I-zone. *Phase V* was assigned to the reperfusion and was associated with arrhythmias encompassing both the I- and C-zones. The occurrence and duration of individual phases as well as representative traces acquired from two regions positioned inside the I- and C-zones are shown in Fig. 4. Visual representation of the events as selected sequential *x-y* frames from individual phases can be seen in Fig. 5 (an online movie file further illustrates this process. See http://ajpheart.physiology.org/cgi/content/full/00381.2003/DC1). A compressed linescan image (complied from 50 sequential 6-s linescans from a representative experiment) allows one to observe the entire process as a continuously evolving sequence of events (Fig. 6). The detailed account of the events associated with each phase is presented in Fig. 7 and is discussed below.

Phase I. Decreasing conduction inside the I-zone. Linescan images of a monolayer acquired at different times after the addition of Iso-Hept and traces from individual sites are shown in Fig. 7*A*. At the macroscopic level (calculated over 1 mm distance), velocity of the propagating CaT wave displayed a smooth exponential decay and reached as low as 1 mm/s. Slowing was quickly followed by a propagation failure. On the level of individual cells, the amplitude of CaT abruptly declined to ~50% of initial CaT value, which was followed by a flat trace. Together, the events during *phase I* were similar to the behavior of the network during the initial stages of Hept experiments (Fig. 2) and lasted 27 ± 5 s.

Phase II. Period of quiescence. Phase I was followed by a short period when no activity was observed within the I-zone (Fig. 7*A*). This quiescent period lasted from 5 to 120 s. As shown in Fig. 2, Hept diminishes gap-junctional conductance almost immediately [it takes ~10 s to establish the flow within the I-zone (4)], whereas it takes >1 min for Iso to affect its intracellular targets (19; and our unpublished data). Therefore, during *phase II*, the wave of excitation caused by the external pacing stimuli fails to penetrate into the I-zone due to an increased intercellular resistance, whereas the excitability of I-zone myocytes has not reached the critical value required for the spontaneous generation of ectopic activity.

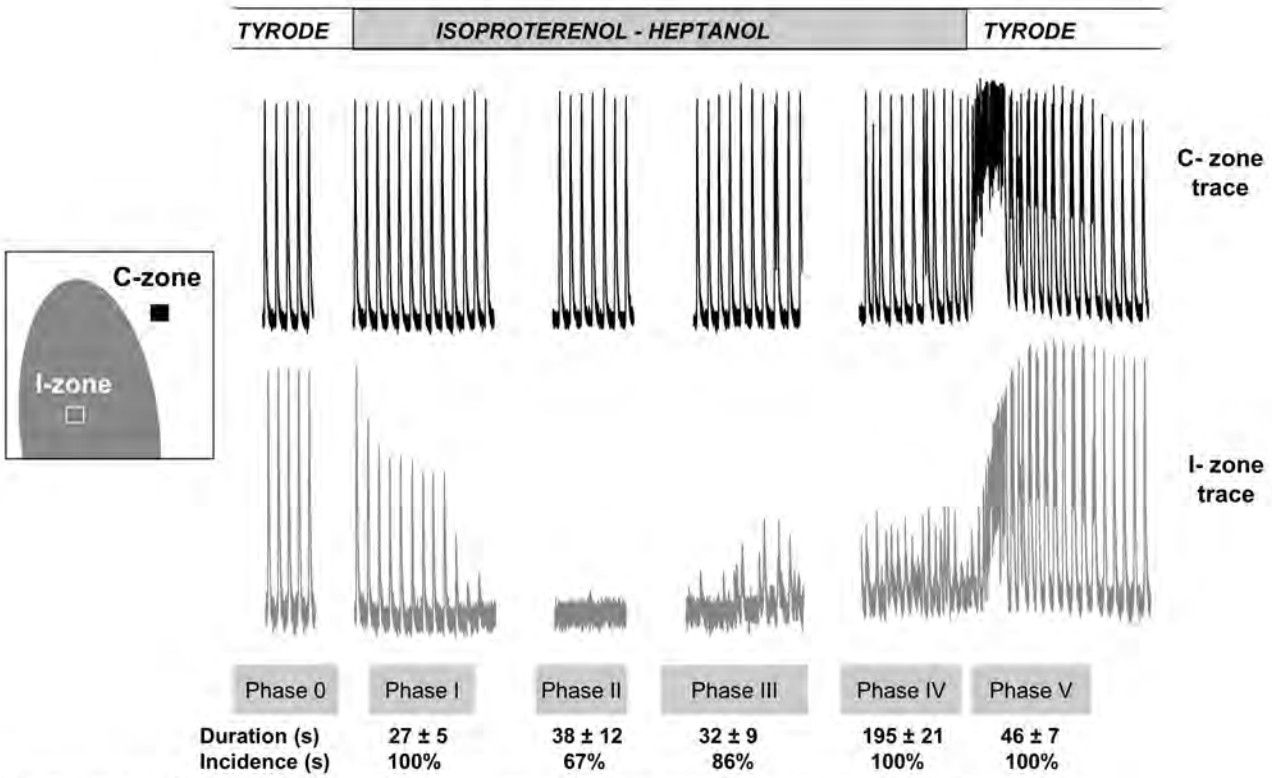

Fig. 4. Perfusion with Hept and isoproterenol (Iso): occurrence of phases and reperfusion arrhythmia. Traces from the representative experiment (gray, I-zone; black, control). *Left*, Regions of interest. *Bottom*: duration and occurrence of individual phases (see text).

Phase III. Appearance of individual CaT and formation of small ectopic clusters. Asynchronous CaT began to appear within I-zone ~50 s after Iso-Hept perfusion was initiated (Fig. 7*B*). The amplitude of CaT was ~50% of their original control values, but CaT temporal features (e.g., duration, $t_{1/2}$ to peak, and $t_{1/2}$ of decay) remained the same. Approximately 100 s into the Iso-Hept perfusion, CaT from individual cells began to trigger CaT in adjacent myocytes (Fig. 7*B*). These events appeared as small asymmetric clusters in which activity was propagated with 0.4–1 mm/s velocity (at the level of few cells the macroscopic velocity of CaT propagation can be only estimated due to its saltatory pattern). Notably, the linescan mode may, to some extent, exaggerate the "saltatory" pattern of cell-to-cell propagation due to the nonlinear arrangement of the cells (as connecting myocytes can lie above or beneath the line). The *phase III* duration ranged from 5 to 30 s.

Phase IV. CaT waves confined to I-zone. Progression of ectopic clusters into CaT waves leads to a complex spatiotemporal pattern of colliding CaT waves (Fig. 7*C*) which is reflected as highly irregular beats on the I-zone trace (Fig. 4). The linear velocity of these waves ranged between 0.4 and 1 mm/s and did not increase significantly during continuous exposure to Iso-Hept. The complex pattern of activity in the I-zone caused no substantial rhythm disturbance to the surrounding control network (Fig. 4). Multiple CaT waves remained confined to the I-zone and failed to trigger CaT in the control area (Fig. 7*C*, *inset*). Therefore two patterns of activity existed independently: across the C-zone, fast, paced CaT waves propagating with a single front; inside the I-zone, disorganized regimes of slow CaT waves with multiple wavebreaks. *Phase IV* persisted as long as the I-zone was perfused with Iso-Hept solution.

Phase V. Events during washout of Iso-Hept containing Tyrode solution. Washout of Iso-Hept led to tachyarrhythmias encompassing the entire myocyte network (Fig. 7*D*). Approximately 10 s after the flow of Iso-Hept was terminated, the CaT waves from the control area began to invade the I-zone (Fig. 7*D*). At the same time, some of the CaT waves originating in the I-zone escaped into the control area. Conduction velocity rapidly rose and the frequency of escaping CaT waves increased. The inhomogeneity on the cellular level led to the escape of the ectopic activity from several areas of the border. If the remaining I-zone was still in a recovery phase, such a scenario often led to a transient reentry-like pattern around the I-zone. Altogether, the mean frequency of CaT increased (from original pacing frequency of 0.4–2.5 Hz) and tachyarrhythmia encompassing both zones was recorded. It typically lasted from 50 to 100 s and was followed by a gradual return to the pacing frequency.

Numerical studies. We hypothesized that the above-described sequence of events is not limited to a specific response of cultured neonatal cardiomyocytes to a local application of Iso-Hept and may occur when part of a cardiac cell network is subjected to conditions that lead

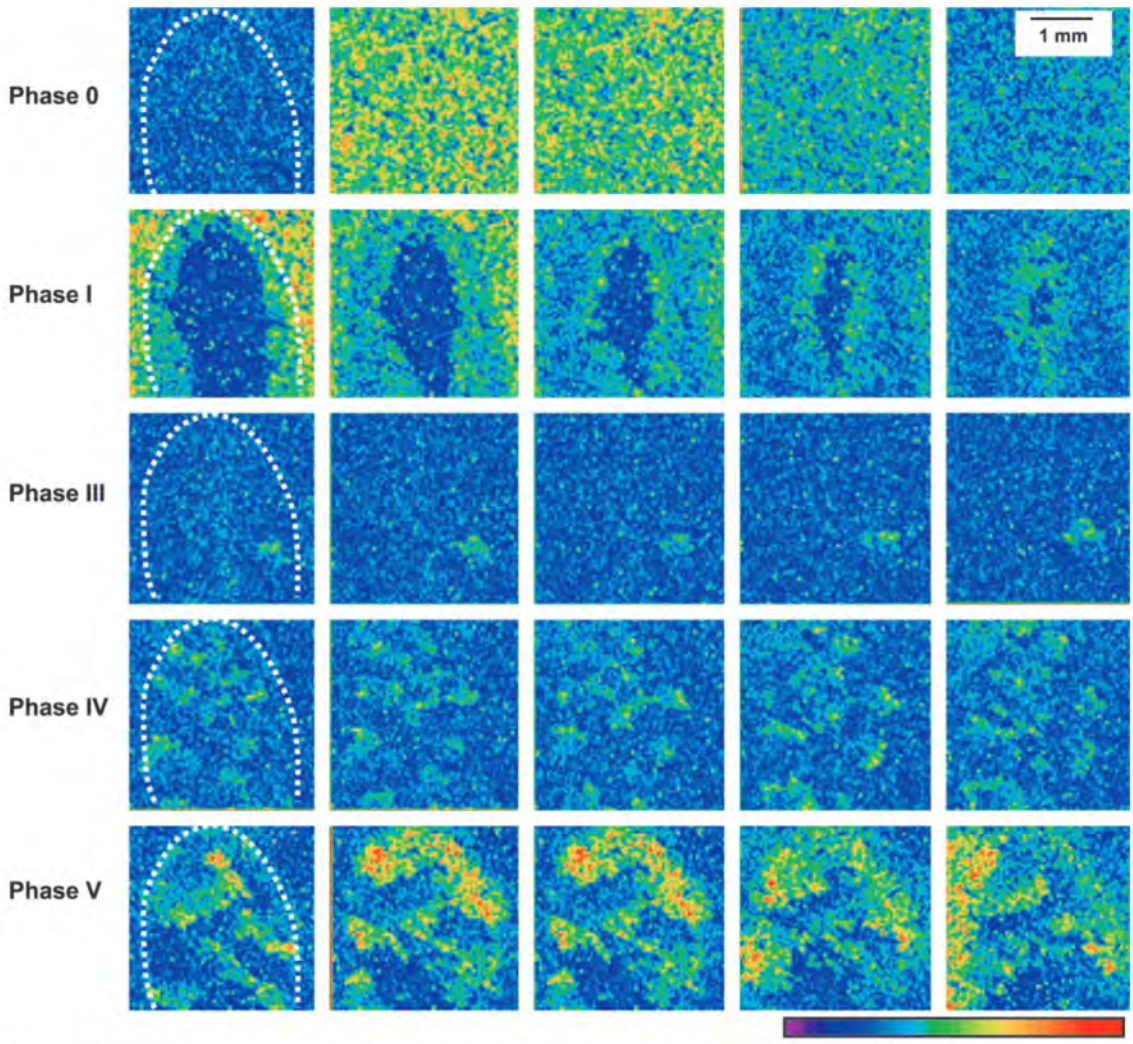

Fig. 5. Appearance of the Iso-Hept-induced events in the *x-y* mode. Each row corresponds to a specific phase (*left*) and consists of five sequential frames. White dotted line shows the site of the I-zone. Pseudocolor corresponds to increasing calcium concentrations. For better visualization of the phases in *x-y* mode, see online supplement at http://ajpheart.physiology.org/cgi/content/full/00381.2003/DC1.

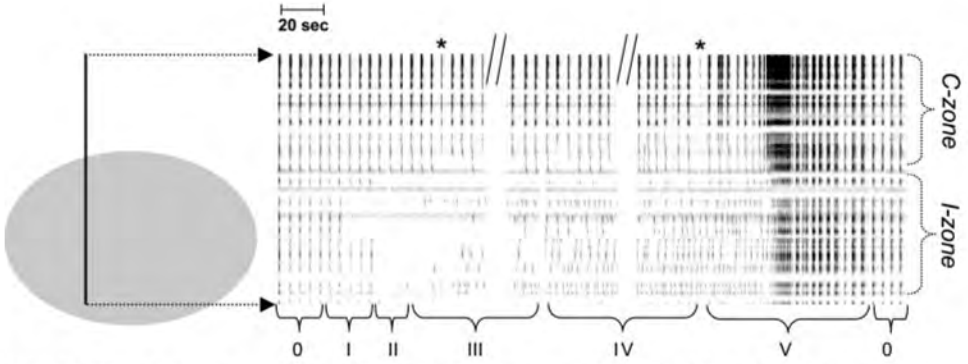

Fig. 6. Appearance of the Iso-Hept-induced events in a *x-t* mode. The diagram shows position of the laser beam used to acquire *x-t* images shown on the right. The compressed linescan image on the right is complied from 50 individual ~6-s long *x-t* frames (each frame consist of 1,024 lines, 6-ms/line). Because of a computer-generated delay between two consecutive *x*-t frames, 0.5-s intervals are present between individual frames. They can be seen as white vertical lines, which in few cases (*) interfere with appearance of the CaTs. The top part of the *x-t* image corresponds to the C-zone (paced CaT, followed by arrhythmia). The bottom part of the *x-t* image corresponds to the I-zone and allows one to visualize all five phases of the ectopic process (details in text).

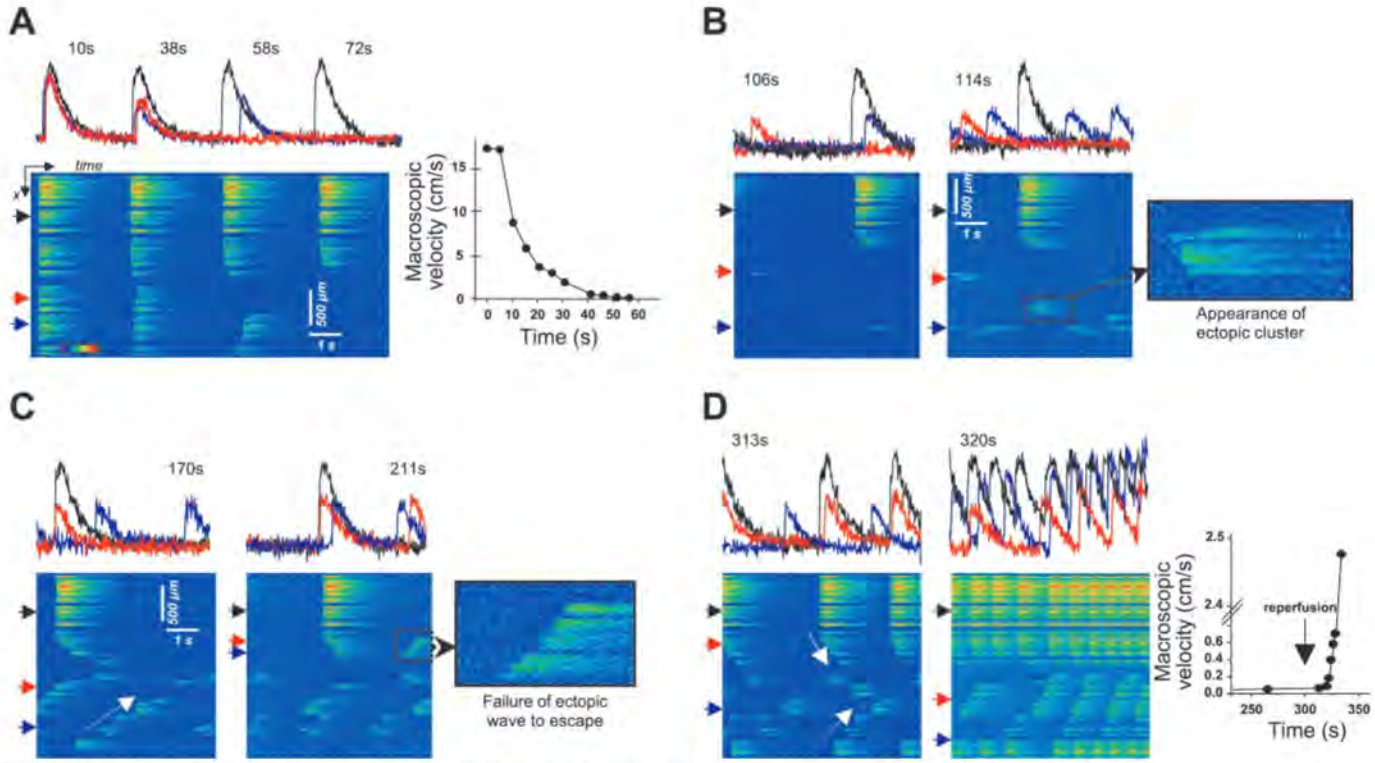

Fig. 7. Individual phases and traces from specific sites as they appear in a *x-t* mode. Position of the scanning line relative to the I-zone was identical to Fig. 6. *A*: phase I, slowing of CaT wave propagation. Representative linescan images show slowing and failure of conduction during initial stages of Iso/Hept application (only the relevant part of *x-t* frames containing CaT are shown). Traces from three specific sites (see arrows) are shown in their respective colors above the linescan images. One can see an almost immediate decline in CaT amplitude and escalating delays between control and I-zone cells. The slope of the CaT wavefront decreases (reflecting diminishing conduction velocity) and saltatory pattern of CaT propagation appears. The linescan image on the right illustrates *phase II* when CaTs were absent from the I-zone. *Right*, changes in velocity of CaT wave propagation within the I-zone. *B*: *phase III*, appearance of ectopics and ectopic clusters. Traces from three specific sites are shown in their respective colors above the linescan images. After a period of silence, individual CaT began to randomly appear. Within seconds they give rise to ectopic clusters (*inset*), visible in linescan mode as 3 to 5 adjacent cells firing within a 50–200 ms from each other (image on the right). While I-zone exhibits a highly disordered pattern of CaTs, the activity in the control area is undisturbed. *C*: *phase IV*, ectopic waves confined to the I-zone. Linescan image at left shows propagation sustained by sequentially activated tissue patches, each of which consists of a few cells being activated simultaneously (dotted white arrow). The frame on the right illustrates entrance/exit block that occurs at the border of the I-zone. The propagating wave of CaT from the control zone slows down and fails to elicit further CaT in the I-zone. On the other hand, the ectopic wave originating within the I-zone (*inset*) fails to activate the control network. Notably, the same myocytes participate in both control and ectopic CaT waves. Overall, the I-zone trace continues to exhibits highly disordered behavior, whereas the activity in the control area is undisturbed. *D*: *phase V*, reperfusion arrhythmia. Washout of ischemic solution was accompanied by the rapid restoration of coupling within the I-zone. Paced CaT from the C-zone started to penetrate into the I-zone (white dotted arrows at left). At the same time, the ectopic CaT from the I-zone escaped into the control zone, leading to the increased frequency of control CaT. Altogether, marked arrhythmia was present in both I- and C-zone. The linescan image on the right demonstrates the increasing slope of the CaT wavefront (which reflects increasing conduction velocity) within the I-zone and disappearance of the saltatory propagation pattern. The reentry-like activity around the I-zone is reflected in an alternating pattern of the CaT recorded from the opposite sides of the control area (black and blue traces). *Right*, rapid restoration of the velocity of CaT propagation within the I-zone.

to a decreased cell-to-cell coupling and increased excitability (allowing individual ventricular-like cells to gain automaticity to various degrees). To test this hypothesis we have chosen a generic FHN model that does not tailor ionic currents to specific values from different species but operates with lump changes in coupling and excitability (see DISCUSSION for justification). Specifically, we employed a 20 × 40 array of FHN-based cardiac cells and modeled effects of Iso and Hept by changing with time the parameter α and the coupling coefficient D, respectively (Fig. 8). These changes induced oscillatory behavior within the I-zone (Fig. 8*B*) and triggered arrhythmogenic process, which proceeded through experimentally observed phases (Fig. 8, *C* and *D*). The events in the I-zone included propagation slowing (e.g., Fig. 8*D*, 30 s), period of quiescence (Fig. 8, 90 s), individual cells firing, and expansion of clusters (Fig. 8*D*, 174 s). It was followed by the development of slow ectopic waves confined to the I-zone (Fig. 8*D*, 294 and 324 s). Reperfusion led to the escape of ectopic waves into the control network (Fig. 8*D*, 432 s). Similar to the experimental findings,

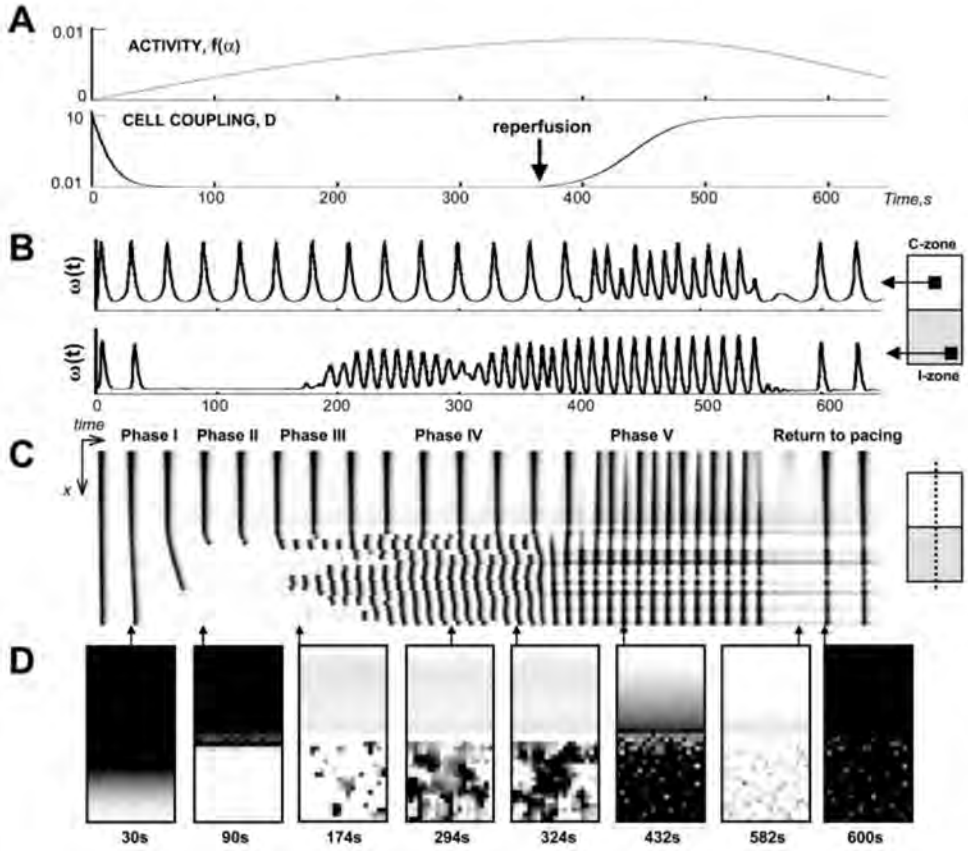

Fig. 8. Results of numerical studies based on FitzHugh-Nagumo model. *A*: time course of the cell excitability (f_α) and cell-coupling coefficient (D) in the I-zone. *B*: traces of activity from the C- and I-zones. In the I-zone, cells start firing before reperfusion, but arrhythmia in the C-zone arrives only after reperfusion and lasts ~100 s. *C*: simulated linescan (at fixed y coordinate, $y = 10$). Time scale is the same as in Fig. 8, *A* and *B*. *Phases I–V* are indicated on the top. It is seen that qualitatively events are identical to the experimentally observed process (compare with Fig. 6). *D*: selected frames from the x-y sequence of events. A gray scale is used, with the convention that an active cell is shown in black, and a resting cell is shown in white. They illustrate the appearance and development of the ectopic activity and wave propagation from the I-zone to the C-zone. The small upward arrows indicate the corresponding times on the linescan image.

paced activity failed to enter the ectopic area during *phases III* and *IV* and the ectopic activity propagated within the I-zone as slow, phasic waves (15). Because we were considering a random distribution of α_0 values, several simulations using different patterns of α_0 were performed. The exact patterns of activity depended on the precise distribution of α_0 in each case, but the general behavior was in good qualitative agreement with the experimental findings (compare Fig. 4 with Fig. 8*B*, Fig. 6 with Fig. 8*D* and Fig. 5 with Fig. 8*C*).

Although a disturbance of the control rhythm is clearly present in simulation traces (Fig. 8*B*), the tachyarrhythmia was much less pronounced in the simulation trace compared with the one obtained experimentally (Fig. 4). One must remember, however, that our modeling studies examined the effects of a small (20 × 20-cell wide) I-zone region on an equally small control area. The size of the experimental I-zone is much larger and covers thousands of cells. Thus multiple ectopic waves escape from the various regions of the border, and their interference creates a more complex tachyarrhythmic pattern in the control network.

DISCUSSION

In our experiments local application and washout of Hept did not disturb paced rhythmic contractions in the surrounding control network (Fig. 2). Another set of experiments has established that the application of 5 μM Iso to a small area of cell network did not, under specified experimental pacing protocol, elicit arrhythmogenic response either during perfusion or Iso washout, despite expected changes in individual CaT dynamics due to known effects of catecholamines on the L-type Ca^{2+} current, Ca^{2+}-induced Ca^{2+} release, and phospholamban phosphorylation (7, 19, 34). Together, these experiments have confirmed that a local increase in excitability or a change in coupling alone does not create conditions that favor formation and spread of ectopic activity. Simulations using the FHN model corroborated this conclusion (data not shown).

When both Iso and Hept were applied to the I-zone (Fig. 4–7), it led to the formation of ectopic waves within the I-zone and reperfusion arrhythmias. Although we divided the observed phenomenon into five phases to assist quantification and description of underlying events, the process was essentially continuous. Notably, it appeared that several protocols tested using our model, including Iso-Hept treatment, washout of ischemia-like solution, multiple ischemic episodes (3), proceeded through similar phases or steps that led to arrhythmia development.

To simulate network behavior we had to choose among a variety of established theoretical models, starting with a generic FHN model, which effectively lumps together the various slow currents (15), to a more detailed Luo-Rudy model, which consider specific ionic currents and their kinetics (22), or even more

recent ones that include local factors, such as dyadic space (12). Our reasons for employing FHN are threefold. First, our main purpose was to understand whether an experimentally observed sequence of events could be a result of concurrent changes in cell excitability and coupling under conditions of cell heterogeneity. We thus did not intend to use modeling to identify contributions from particular ionic currents (which is an arguably important but different issue). On the contrary, the fact that lumped changes in excitability and coupling (under condition of cell heterogeneity) are sufficient to describe the progression of ectopic activity from an injury area to the surrounding control network, suggest that this phenomenon may occur in a broad range of excitable tissues and is not limited to a network of neonatal rat cells. Second, the FHN model allowed us to simulate the behavior of a 2D lattice of heterogeneous cells. The use of detailed models would make our studies computationally unnecessarily costly without answering our original question. Finally, because the exact values, relative abundance of particular channels, and Iso-induced changes to specific ionic currents (a variety of currents are known to be affected by Iso and their relative contribution to increased cells excitability remain controversial) had to be derived from disparate data on different species and would have been entirely arbitrary, the likelihood of providing physiologically relevant insights using more detailed models of cardiac cells would have been negligible at this stage.

The computational approach has confirmed that the observed scenario can be reproduced by assuming a change in two macroscopic parameters: cell-to-cell coupling and depolarization rate, the latter being random. We emphasize the importance of the random nature of the activity. Specifically, the patterns shown in Fig. 8 correspond to a random Gaussian distribution of "slopes," whereas the system of identical cells does not generate waves of activity, but instead oscillates uniformly in the I-zone (data not shown). The problem of coupled oscillatory waves has been investigated in the past, in particular in the context of pacemaker activity in the sinoatrial node (25). In the case of well-coupled cells, where the heterogeneities in the period of oscillation are small, the dynamics of the system can be understood by using standard mathematical methods (15): the system oscillates as a whole; all cells are synchronized. In a weakly coupled case considered in this study, nontrivial spatiotemporal patterns of activities corresponding to slow waves of synchronization ("phase waves," see Ref. 15) are observed. In larger systems, as it happens in the experiment it leads to an apparently chaotic regime (Fig. 4). Importantly, disorganized regimes appear only when the dispersion of periods is large enough and the coupling between cells is small enough. Increasing the coupling, and/or decreasing the dispersion of frequencies of the cells, results in a better synchronization and in more regular regimes. Decreasing the number of oscillatory cells also results in more ordered regimes. A consequence of the low coupling between the cells in the I-zone is that the phase waves are slow, as observed experimentally and numerically. The numerically observed wave velocity drops by a factor ~30 when the diffusion constant is reduced by a factor of 1,000, consistent with general results (15), and in qualitative agreement with the experimental data (Fig. 7*A*).

Our protocol generates a network of weakly coupled, pacemaker-like cells (I-zone) surrounded by the ventricular-type cells paced by the external source (C-zone). Experimental traces from the I-zone and the C-zone reveals an independent pattern of activity inside each zone during *phases III* and *IV*. Simulations using the FHN model have also shown that when the diffusion coefficients in the I-zone and the C-zone are sufficiently different (by >2 orders of magnitude), the I-zone waves are unable to trigger activity on the ventricular side and vice versa.

For individual ectopic foci, this situation and its relationship to coupling are often referred as protected loci or exit/entrance block (30, 35). The novelty of our results derives from a combination of an entrance/exit block concept (failure of CaT waves to enter and exit the ectopic area) with two other factors: network heterogeneity and spatial (2D) arrangement of many ectopic cells. Together these conditions led to multiple ectopic waves confined to the affected area.

The large discrepancy between the coupling constants in the two zones is responsible for the lack of propagation from one zone to the other. Making the two coupling constants closer renders propagation to and from the I-zone possible. During the reperfusion phase this effect is observed and is at the origin of the extra beats observed in Fig. 8 in the C-zone in the time interval t = 400–550 s.

Our experiments and simulations dealt with a 2D network of cardiac cells. Myocardium, on the other hand, is a 3D structure, and further studies will be required to extend our conclusions to the 3D case. We suggest, however, that in vivo ectopic events can also occur in a 2D-like environment. Specifically, we hypothesize that an ectopically active layer of cells can be formed from reversibly injured ventricular cardiomyocytes sandwiched between healthy tissue and an irreversibly injured ischemic core. This layer of cells is often referred to as a functional border of the infarcted area (23). Catecholamine surge and/or calcium overload due to microreperfusion (metabolic vasodilatation of neighboring coronary vessel, see Ref. 3) allow the functional border's cells to gain automaticity, i.e., become ectopically active]. Ischemic environment impairs cell-to-cell coupling. We hypothesize that a combination of intrinsic cell heterogeneity, low coupling, and gained automaticity may convert at least a small part of this border cell layer into a semi-2D functional network that exhibits *phase IV* behavior. We named this hypothetical layer an ectopic surface.

If an ectopic surface does exist in vivo, it may affect a relationship between frequency of ectopic loci and its ability to cause arrhythmia in the control network. In contrast to a classic scenario, frequencies of individual ectopic foci do not have to exceed external pacing fre-

quency or be time matched to avoid refractoriness of the surrounding tissue. Indeed, the existence of the ectopic surface implies an essentially constant source of activation for the control network due to an added spatial component (e.g., ectopic waves "whirl" continuously within the ectopic surface). During ischemia-like conditions, the coupling gradient prevents exit of ectopic waves into the surrounding tissue. Reperfusion brings recovery of gap-junctional conductance across the border. Inevitably, ectopic waves propagating alongside the border escape at the first spot where conditions of exit block (e.g., uncoupling and refractoriness) are relieved. Thus, in the presence of an ectopic surface, arrhythmogenesis is not directly related to the frequency of individual ectopic cells and their paced counterparts. The same reasoning implies that the existence of an ectopic surface will substantially widen the "vulnerability window" required for reentry formation (32).

In conclusion, our experimental and theoretical studies have suggested a sequence of events that may allow for the ectopic activity to develop into an arrhythmia. Specifically, our data indicate the following: *1*) local part of a ventricular network gains pacemaker-like properties in the presence of β-adrenergic stimulation; *2*) because of the intrinsic cell heterogeneity and low coupling, induced by gap junction uncoupler, slow ectopic waves develop within the injured zone; *3*) the ventricular (paced) and injured (ectopically active) part of the network exhibit independent patterns of activity; and *4*) on recovery of cell-to-cell coupling between the control and injured area, ectopic waves exit at multiple sites of the injured area's border, creating a disorganized wave pattern and arrhythmia in the control network.

The authors are grateful to Ariel Escobar for valuable discussions.

DISCLOSURES

This study was supported by the National American Heart Association Established Investigator Award (to N. Sarvazyan).

REFERENCES

1. **Akar FG, Roth BJ, and Rosenbaum DS.** Optical measurement of cell-to-cell coupling in intact heart using subthreshold electrical stimulation. *Am J Physiol Heart Circ Physiol* 281: H533–H542, 2001.
2. **Akiyama T, Yamazaki T, and Ninomiya I.** Differential regional responses of myocardial interstitial noradrenaline levels to coronary occlusion. *Cardiovasc Res* 27: 817–822, 1993.
3. **Arutunyan A, Swift LM, and Sarvazyan N.** Initiation and propagation of ectopic waves: insights from an in vitro model of ischemia-reperfusion injury. *Am J Physiol Heart Circ Physiol* 283: H741–H749, 2002.
4. **Arutunyan A, Webster DR, Swift LM, and Sarvazyan N.** Localized injury in cardiomyocyte network: a new experimental model of ischemia-reperfusion arrhythmias. *Am J Physiol Heart Circ Physiol* 280: H1905–H1915, 2001.
5. **Bastide B, Herve JC, Cronier L, and Deleze J.** Rapid onset and calcium independence of the gap junction uncoupling induced by heptanol in cultured heart cells. *Pflügers Arch* 429: 386–393, 1995.
6. **Beardslee MA, Lerner DL, Tadros PN, Laing JG, Beyer EC, Yamada KA, Kleber AG, Schuessler RB, and Saffitz JE.** Dephosphorylation and intracellular redistribution of ventricular connexin43 during electrical uncoupling induced by ischemia. *Circ Res* 87: 656–662, 2000.
7. **Bers DM.** Ca regulation in cardiac muscle. *Med Sci Sports Exerc* 23: 1157–1162, 1991.
8. **Bub G, Shrier A, and Glass L.** Spiral wave generation in heterogeneous excitable media. *Physiol Rev Lett* 88: 058101, 2002.
9. **Burt JM, Massey KD, and Minnich BN.** Uncoupling of cardiac cells by fatty acids: structure-activity relationships. *Am J Physiol Cell Physiol* 260: C439–C448, 1991.
10. **Carmeliet E.** Cardiac ionic currents and acute ischemia: from channels to arrhythmias. *Physiol Rev* 79: 917–1017, 1999.
11. **Dekker LR, Rademaker H, Vermeulen JT, Opthof T, Coronel R, Spaan JA, and Janse MJ.** Cellular uncoupling during ischemia in hypertrophied and failing rabbit ventricular myocardium: effects of preconditioning. *Circulation* 97: 1724–1730, 1998.
12. **Greenstein JL and Winslow RL.** An integrative model of the cardiac ventricular myocyte incorporating local control of Ca^{2+} release. *Biophys J* 83: 2918–2945, 2002.
13. **Joyner RW and van Capelle FJ.** Propagation through electrically coupled cells. How a small SA node drives a large atrium. *Biophys J* 50: 1157–1164, 1986.
14. **Joyner RW, Wang YG, Wilders R, Golod DA, Wagner MB, Kumar R, and Goolsby WN.** A spontaneously active focus drives a model atrial sheet more easily than a model ventricular sheet. *Am J Physiol Heart Circ Physiol* 279: H752–H763, 2000.
15. **Keener J and Sneyd J.** *Mathematical Physiology*. New York: Springer Verlag, 1998.
16. **Kimura H, Oyamada Y, Ohshika H, Mori M, and Oyamada M.** Reversible inhibition of gap junctional intercellular communication, synchronous contraction, and synchronism of intracellular Ca^{2+} fluctuation in cultured neonatal rat cardiac myocytes by heptanol. *Exp Cell Res* 220: 348–356, 1995.
17. **Kumar NM and Gilula NB.** The gap junction communication channel. *Cell* 84: 381–388, 1996.
18. **Kumar R, Wilders R, Joyner RW, Jongsma HJ, Verheijck EE, Golod DA, van Ginneken AC, and Goolsby WN.** Experimental model for an ectopic focus coupled to ventricular cells. *Circulation* 94: 833–841, 1996.
19. **Kuznetsov V, Pak E, Robinson RB, and Steinberg SF.** β_2-Adrenergic receptor actions in neonatal and adult rat ventricular myocytes. *Circ Res* 76: 40–52, 1995.
20. **Lameris TW, de Zeeuw S, Alberts G, Boomsma F, Duncker DJ, Verdouw PD, Veld AJ, and van Den Meiracker AH.** Time course and mechanism of myocardial catecholamine release during transient ischemia in vivo. *Circulation* 101: 2645–2650, 2000.
21. **Laurita KR and Singal A.** Mapping action potentials and calcium transients simultaneously from the intact heart. *Am J Physiol Heart Circ Physiol* 280: H2053–H2060, 2001.
22. **Luo CH and Rudy Y.** A dynamic model of the cardiac ventricular action potential. I. Simulations of ionic currents and concentration changes. *Circ Res* 74: 1071–1096, 1994.
23. **McCulloch AD and Mazhari R.** Regional myocardial mechanics: integrative computational models of flow-function relations. *J Nucl Cardiol* 8: 506–519, 2001.
24. **McHowat J, Yamada KA, Wu J, Yan GX, and Corr PB.** Recent insights pertaining to sarcolemmal phospholipid alterations underlying arrhythmogenesis in the ischemic heart. *J Cardiovasc Electrophysiol* 4: 288–310, 1993.
25. **Michaels DC, Chialvo DR, Matyas EP, and Jalife J.** Dynamics of synchronization in the sinoatrial node. *Ann NY Acad Sci* 591: 154–165, 1990.
26. **Pollard AE, Cascio WE, Fast VG, and Knisley SB.** Modulation of triggered activity by uncoupling in the ischemic border. A model study with phase 1b-like conditions. *Cardiovasc Res* 56: 381–392, 2002.
27. **Press W, Teukolsky S, Vetterling W, and Flannery B.** *Numerical Recipes*. New York: Cambridge University Press, 1992.
28. **Rohr S, Kucera JP, Fast VG, and Kleber AG.** Paradoxical improvement of impulse conduction in cardiac tissue by partial cellular uncoupling. *Science* 275: 841–844, 1997.

29. **Rohr S and Salzberg BM.** Multiple site optical recording of transmembrane voltage (MSORTV) in patterned growth heart cell cultures: assessing electrical behavior, with microsecond resolution, on a cellular and subcellular scale. *Biophys J* 67: 1301–1315, 1994.
30. **Rosenthal JE and Ferrier GR.** Contribution of variable entrance and exit block in protected foci to arrhythmogenesis in isolated ventricular tissues. *Circulation* 67: 1–8, 1983.
31. **Shaw RM and Rudy Y.** Ionic mechanisms of propagation in cardiac tissue. Roles of the sodium and L-type calcium currents during reduced excitability and decreased gap junction coupling. *Circ Res* 81: 727–741, 1997.
32. **Starmer CF, Biktashev VN, Romashko DN, Stepanov MR, Makarova ON, and Krinsky VI.** Vulnerability in an excitable medium: analytical and numerical studies of initiating unidirectional propagation. *Biophys J* 65: 1775–1787, 1993.
33. **Takens-Kwak BR, Jongsma HJ, Rook MB, and Van Ginneken AC.** Mechanism of heptanol-induced uncoupling of cardiac gap junctions: a perforated patch-clamp study. *Am J Physiol Cell Physiol* 262: C1531–C1538, 1992.
34. **Viatchenko-Karpinski S and Gyorke S.** Modulation of the Ca^{2+}-induced Ca^{2+} release cascade by β-adrenergic stimulation in rat ventricular myocytes. *J Physiol* 533: 837–848, 2001.
35. **Wagner MB, Golod D, Wilders R, Verheijck EE, Joyner RW, Kumar R, Jongsma HJ, Van Ginneken AC, and Goolsby WN.** Modulation of propagation from an ectopic focus by electrical load and by extracellular potassium. *Am J Physiol Heart Circ Physiol* 272: H1759–H1769, 1997.
36. **Wang Y and Rudy Y.** Action potential propagation in inhomogeneous cardiac tissue: safety factor considerations and ionic mechanism. *Am J Physiol Heart Circ Physiol* 278: H1019–H1029, 2000.
37. **Wilders R, Wagner MB, Golod DA, Kumar R, Wang YG, Goolsby WN, Joyner RW, and Jongsma HJ.** Effects of anisotropy on the development of cardiac arrhythmias associated with focal activity. *Pflügers Arch* 441: 301–312, 2000.
38. **Yamada KA, McHowat J, Yan GX, Donahue K, Peirick J, Kleber AG, and Corr PB.** Cellular uncoupling induced by accumulation of long-chain acylcarnitine during ischemia. *Circ Res* 74: 83–95, 1994.
39. **Zeng J and Rudy Y.** Early afterdepolarizations in cardiac myocytes: mechanism and rate dependence. *Biophys J* 68: 949–964, 1995.